Available online at www.sciencedirect.com
SCIENCE DIRECT®
ELSEVIER
Earth and Planetary Science Letters 220 (2004) 139–155
EPSL
www.elsevier.com/locate/epsl

Origin of adakitic intrusives generated during mid-Miocene east–west extension in southern Tibet

Z.-Q. Hou [a,*], Y.-F. Gao [b], X.-M. Qu [a], Z.-Y. Rui [a], X.-X. Mo [c]

[a] *Institute of Mineral Resources, Chinese Academy of Geological Sciences, Beijing 100037, PR China*
[b] *Shijiazhuang College of Economy, Shijiazhuang, Hebei, PR China*
[c] *China University of Geosciences, Beijing 100082, PR China*

Received 19 June 2003; received in revised form 20 October 2003; accepted 23 December 2003

Abstract

Adakite is an intermediate to felsic rock with low K, high Al, Na and Sr, and depleted in Y and HREE, usually occurring in arc settings related to subduction of an oceanic slab. Here we report the occurrence of potassic adakites from south Tibet in an orogenic belt produced by the Indo–Asian continent collision. These adakitic intrusives, as a product of Neogene east–west extension, occur in a Miocene Cu-bearing porphyry belt, which developed along the Gangdese arc paralleling the Yarlung–Zangbo suture, but is locally controlled by NS-striking normal faulting systems. Available age data define a duration of magmatism of 10–18 Ma for the adakitic intrusives and related extrusive analogues in south Tibet, which occur in a post-collisional extensional setting. Geochemical data indicate that these adakitic intrusives are shoshonitic and exhibit calc-alkaline composition with high K, and high Sr/Y and La/Y coupled with low Y and HREE, similar to adakites derived from slab melting. However, a wide range for $\varepsilon_{Nd(t)}$ (−6.18 to +5.52), initial $^{87}Sr/^{86}Sr$ (0.7049–0.7079), $^{207}Pb/^{204}Pb$ (15.502–15.626), and $^{208}Pb/^{204}Pb$ (38.389–38.960), as well as high K_2O contents (2.6–8.6 wt%) and relatively high Mg# values (0.32–0.74) indicate that these adakitic magmas were formed by a complex mechanism involving partial melting of mafic materials in a thickened lower crust with input of enriched mantle and/or upper crust components. Absence of a negative Eu anomaly, extreme depletion in Y, Nb and Ti, and variable high Sr/Y and La/Yb ratios suggest that the lower crustal source is probably a hydrous amphibole eclogite or garnet amphibolite, as exhumed in the western and eastern Himalayan syntaxes on the Tibetan plateau. Partial melting of the lower crust was most likely triggered by mantle-derived ultra-potassic magmatism (17–25 Ma) formed by slab breakoff or mantle thinning. During the formation and migration of pristine adakitic melts, additional input of ultra-potassic magmas and upper crustal materials could account for the observed ε_{Nd}–ε_{Sr} signatures and high Rb/Sr, K and Mg# characteristics for most of the adakitic intrusives in south Tibet.

Keywords: potassic Cu porphyry; adakitic intrusives; lower crust melting; south Tibet

1. Introduction

Defant and Drummond [1,2] published significant works on adakite, a special rock with composition characterized by low K, high Al, Na and

* Corresponding author.
E-mail address: hzq@cags.en.net (Z.-Q. Hou).

0012-821X/04/$ – see front matter © 2004 Published by Elsevier B.V.
doi:10.1016/S0012-821X(04)00007-X

Sr, and depleted in Y and heavy rare earth elements (HREE). Their research has received widespread attention because of its contribution to the understanding of crust–mantle interactions, geodynamic regimes and evaluation of mineral resource potential in convergent margins. Many models for adakite generation have been proposed, such as partial melting of the oceanic slab related to incipient subduction [1–4] or flat subduction [5,6], partial melting of basaltic lower crust [7–11], and assimilation–fractional crystallization (AFC) processes [12]. Experimental studies have also shown that basaltic materials can melt to produce an adakitic melt at pressures equivalent to a crustal thickness of >40 km [13]. Most of the Na-rich adakites in subduction zones, whether their source is slab or lower crust, have been widely investigated, whereas the occurrence of potassic adakitic rocks in continental collision environments is poorly understood.

In the Tibetan–Himalayan orogen, we recently discovered many potassic magma intrusions comprising a Miocene Cu-bearing porphyry belt [14,15], which developed on the Gangdese arc in southern Tibet (Fig. 1). These intrusive rocks show a geochemical affinity with adakite [16,17]. This paper presents new data on the geology and geochemistry of these adakitic intrusive groups, and combined with previous data on Miocene potassic and ultra-potassic volcanic rocks in south Tibet, discusses their origin and significance for geodynamic processes.

2. Geological setting

A characteristic feature of the Neogene tectonism and magmatism in south Tibet is an east–west extension that formed NS-striking normal faulting systems and an associated 1500 km long, post-collisional potassic–ultra-potassic magmatic belt. This belt formed during the Miocene and runs parallel to the Yarlung–Zangbo suture [15,18–20] in south Tibet (Fig. 1a). It connects westward to the Neogene potassic magmatic belt in the South Karakorum [21], and is bounded in the east by a large-scale strike-slip belt and NW-directed Paleocene potassic magmatic belt in eastern Tibet [22,23]. The Miocene potassic magmatic belt defines a later, significant thermal event distinct from the oceanic slab subduction-related magmatisms, which terminated around 40 Ma.

The Gangdese adakitic intrusives within the potassic magmatic belt were developed on the Gangdese arc batholiths, and resulted from the northward subduction of the Neotethyan ocean plate during the Cretaceous [24]. These intrusives constitute an east–west-trending 350 km long porphyry belt in the Lhasa terrane (Fig. 1b). Although the terrane was shortened by about 180 km as a result of the Qiangtang–Lhasa terrane collision during the Jurassic–Cretaceous [25], several tectonic units, i.e., the Indus–Yarlung–Zangbo suture, the Xigaze fore-arc basin [26], and the Gangdese arc granite batholiths [27], are well preserved along the southern margin of the terrane (Fig. 1b). The Gangdese batholiths have a long duration (120–30 Ma) of magmatism, with activity peaking at 110–70 Ma and 55–45 Ma [28]. These timings correspond to that of large-scale subduction of Neotethyan oceanic slab [27] and of the strong collision between the Indian and Asian continents (50–55 Ma), respectively. Northward thrusting followed the syn-collisional magmatism to form the Gangdese central thrust zone at 30–24 Ma [29] and to cause the exhumation of granitic batholiths. A general cooling of the batholiths at around 21 Ma [30] suggests that the rapid rise of the Gangdese arc took place at this time (>2 mm/yr; [30,31]). A series of NS-striking normal faulting systems, resulting from the east–west extension, were developed across the Lhasa terrane (Fig. 1a). Available age data suggest the normal faulting occurred before 13.5–14 Ma [33,34], however, recent $^{40}Ar/^{39}Ar$ dates on the NS-trending ultra-potassic dykes (13–18 Ma [20,32]) indicate that the initial east–west stretching probably took place at approximately 18 Ma [20].

The Gangdese adakitic rocks intruded the granitic batholiths and meta-sedimentary formations and occur as stocks <1 km^2 in an east–west-trending porphyry belt. However, some of them locally appear as small-volume intrusive groups, which cluster within the graben basins and trend for 50 km along the NS-striking normal faulting systems (Fig. 1b). This suggests the control of

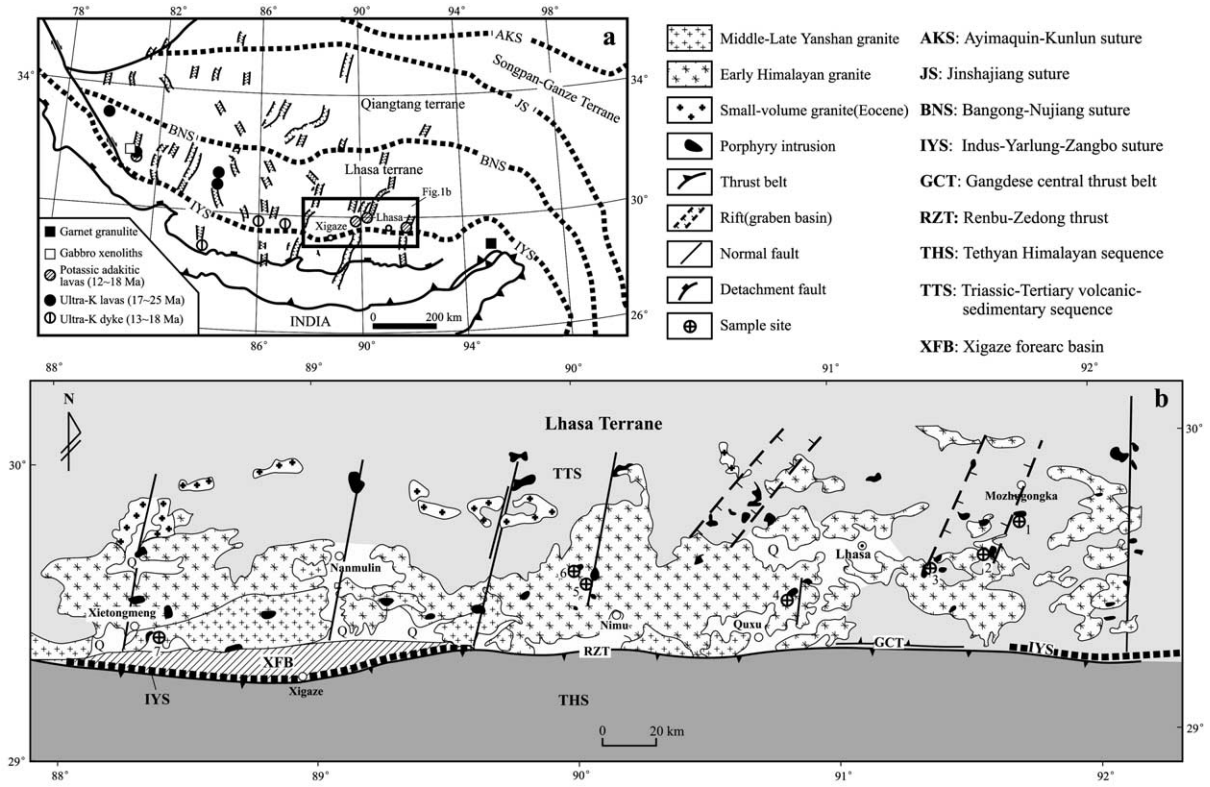

Fig. 1. Simplified tectonic framework of the Himalayan–Tibetan orogen (a) and sketch map of the Gangdese adakitic intrusive belt in south Tibet (b). Panel a shows that NS-striking normal faulting systems controlled the localization of the Miocene adakitic extrusive rocks [18,19,20]. Panel b shows the adakitic intrusive groups intruded the Gangdese arc batholiths in south Tibet. Sample sites: 1-Jiama; 2-Qulong; 3-Lakang'e; 4-Nanmu; 5-Tinggong (Nimu); 6-Chongjiang (Nimu); 7-Dongga.

normal faulting due to east–west extension related to the localization of the adakitic magmatism in south Tibet. Corresponding eruptive facies of the adakitic intrusives have also been observed in the Maquiang [19] and Gazacun [35], ~100 km west of Lhasa, in the S Gegar and SE Barga [18], and in the western part of the Gangdese arc (Fig. 1). These potassic calc-alkaline lavas were also controlled by the NS-striking normal fault systems, and were spatially associated with the Miocene ultra-potassic volcanic rocks in southern Tibet [18].

3. Age results

The Gangdese adakitic intrusives and corresponding extrusive rocks have been dated by various isotopic methods. In order to obtain an accurate age of the adakitic intrusives, three samples from Qulong and Chongjiang were dated using single zircon U–Pb dating by the SHRIMP II at the Chinese Academy of Geological Science (Beijing).

Zircons separated from these adakitic intrusives were documented with transmitted and reflected light micrographs and back-scattered electron images, and the mount was vacuum-coated with a 500 nm layer of high-purity gold. Operating and data processing procedures follow those established in RSES, Australian National University. Transmission electron microscopy (TEM) standard zircon with $^{206}Pb/^{238}U = 0.0668$ at 417 Ma was used for measurements of U–Th abundance and U–Pb–Th isotopic ratios. The uncertainties of individual analyses are reported at the 1σ level

Table 1
SHRIMP U–Pb dating data of zircon from adakitic intrusives in south Tibet

Sample	U (ppm)	Th (ppm)	Th/U	$^{206}Pb^*$ (ppm)	$^{232}Th/^{238}U$	$^{207}Pb^*/^{235}U$ ($\pm 1\sigma$)	$^{206}Pb/^{238}U$ ($\pm 1\sigma$)	Error correlation	$^{206}Pb/^{238}U$ (Ma, 1σ)
Qulong adakitic intrusives									
QZK001-1.1	2088	1174	0.56	5.54	0.58	0.0201 ± 0.0032	0.00294 ± 0.00005	0.103	18.95 ± 0.32
QZK001-3.1	379	263	0.69	0.99	0.72		0.00260 ± 0.00019		16.70 ± 1.20
QZK001-4.1	509	241	0.47	1.26	0.49		0.00238 ± 0.00011		15.32 ± 0.72
QZK001-5.1	468	223	0.48	1.26	0.49	0.0260 ± 0.0125	0.00282 ± 0.00012	0.091	18.17 ± 079
QZK001-6.1	770	1028	1.34	1.89	1.38		0.00268 ± 0.00007		17.26 ± 0.45
QZK001-8.1	427	620	1.45	1.01	1.50	0.0134 ± 0.0054	0.00264 ± 0.00007	0.066	16.96 ± 0.44
QZK001-7.1	312	170	0.54	0.82	0.56		0.00244 ± 0.00023		15.70 ± 1.50
QZK001-9.1	532	855	1.61	1.34	1.66		0.00247 ± 0.00012		15.91 ± 0.76
QZK001-10.1	297	155	0.52	0.87	0.54		0.00266 ± 0.00019		17.10 ± 1.20
QZK001-11.1	203	76	0.37	0.62	0.38		0.00262 ± 0.00026		16.90 ± 1.00
QZK001-12.1	262	303	1.16	0.74	1.19	0.0620 ± 0.0155	0.00279 ± 0.00016	0.233	18.00 ± 1.00
QZK001-12.2	763	1377	1.80	1.88	1.87	0.3160 ± 0.0853	0.00269 ± 0.00016	0.118	17.33 ± 0.54
Weighted mean of 12 points (2σ)									17.68 ± 0.74
Chongjiang adakitic intrusives									
CZK051-26-1.1	438	331	0.76	1.01	0.78		0.00223 ± 0.00016		14.30 ± 1.00
CZK051-26-2.1	505	523	1.04	1.25	1.07	0.0420 ± 0.0105	0.00274 ± 0.00010	0.151	17.62 ± 0.66
CZK051-26-3.1	448	331	0.74	1.09	0.76		0.02380 ± 0.00131		15.34 ± 0.85
CZK051-26-5.1	840	1519	1.81	1.86	1.87	0.1710 ± 0.0731	0.00235 ± 0.00007	0.067	15.12 ± 0.45
CZK051-26-6.1	253	153	0.60	0.61	0.63	0.0350 ± 0.0133	0.00230 ± 0.00013	0.149	14.80 ± 0.84
CZK051-26-7.1	974	1110	1.14	2.16	1.18	0.2120 ± 0.0657	0.00241 ± 0.00007	0.094	15.54 ± 0.46
CZK051-26-8.1	605	640	1.06	1.33	1.03	0.0164 ± 0.0100	0.00230 ± 0.00010	0.070	15.79 ± 0.63
CZK051-26-9.1	592	439	0.74	1.43	0.77		0.00223 ± 0.00013		14.38 ± 0.86
CZK051-26-10.1	718	1090	1.52	1.70	1.57	0.0307 ± 0.0077	0.00257 ± 0.00007	0.115	16.51 ± 0.48
CZK051-26-11.1	491	409	0.83	1.17	0.86		0.00224 ± 0.00014		14.42 ± 0.89
CZK051-26-13.1	643	734	1.14	1.43	1.18	0.0267 ± 0.0067	0.00245 ± 0.00007	0.111	15.74 ± 0.44
CZK051-26-14.1	484	311	0.64	1.08	0.66	0.0217 ± 0.0080	0.00239 ± 0.00008	0.096	15.36 ± 0.54
CZK051-26-15.1	554	542	0.98	1.33	1.01		0.00257 ± 0.00011	0.433	16.55 ± 0.67
Weighted mean of 13 points (2σ)									15.60 ± 0.52
Chongjiang adakitic intrusives									
CZK051-470-2.1	4365	9351	2.14	9.90	2.21	0.0175 ± 0.0009	0.00262 ± 0.00006	0.442	16.84 ± 0.41
CZK051-470-3.1	1018	807	0.79	2.03	0.82	0.0275 ± 0.0025	0.00232 ± 0.00008	0.336	14.91 ± 0.49
CZK051-470-4.1	786	395	0.50	1.47	0.52	0.0212 ± 0.0066	0.00202 ± 0.00008	0.135	13.02 ± 0.54
CZK051-470-6.1	266	215	0.81	0.65	0.83	0.0688 ± 0.0056	0.00286 ± 0.00012	0.531	18.38 ± 0.79
CZK051-470-7.1	981	1072	1.09	1.84	1.13	0.0160 ± 0.0040	0.00210 ± 0.00006	0.131	13.49 ± 0.44
CZK051-470-9.1	869	939	1.08	1.84	1.12	0.0184 ± 0.0040	0.00238 ± 0.00010	0.187	15.33 ± 0.63
CZK051-470-11.1	999	874		1.95	0.90	0.0188 ± 0.0058	0.00215 ± 0.00010	0.151	13.81 ± 0.64
CZK051-470-12.1	461	256		1.00	0.57	0.0401 ± 0.0076	0.00236 ± 0.00009	0.202	15.18 ± 057
CZK051-470-13.1	475	1025		1.18	2.23		0.00254 ± 0.00014		16.36 ± 0.89
CZK051-470-14.1	625	609		1.01	1.32	0.01 36 ± 0.0087	0.00227 ± 0.00010	0.068	14.61 ± 0.63
CZK051-470-15.1	1251	1793		2.40	1.48	0.0268 ± 0.0064	0.00215 ± 0.00007	0.140	13.82 ± 0.46
CZK051-470-16.1	862	1137		1.70	1.36	0.0526 ± 0.0028	0.00230 ± 0.00006	0.506	14.78 ± 0.40
CZK051-470-17.1	559	490		1.24	0.90		0.00213 ± 0.00013		13.74 ± 0.86
CZK051-470-18.1	491	322		1.06	0.68	0.0143 ± 0.0074	0.00223 ± 0.00009	0.080	14.36 ± 0.59
CZK051-470-19.1	477	220		0.99	0.48	0. 0340 ± 0.0136	0.00224 ± 0.00013	0.146	14.42 ± 0.85
CZK051-470-23.1	421	337		1.01	0.83	0.0230 ± 0.0166	0.00242 ± 0.00015	0.084	15.60 ± 0.94
Weighted mean of 16 points (2σ)									14.54 ± 0.65

U–Pb dating was conducted at the Chinese Academy of Geological Science (Beijing) using SHRIMP II. The uncertainties of individual analyses are reported at the 1σ level. The mean dates for $^{206}Pb/^{238}U$ analyses are used to indicate crystallization age of adakitic magmas, with 95% confidence interval (2σ). Operating and data processing procedures follow those established in RSES, Australian National University. Standard material for measurements of U–Th abundance and U–Pb–Th isotopic ratios of analyzed samples is TEM standard zircon with $^{206}Pb/^{238}U = 0.0668$ at 417 Ma. The mass resolution used for determining Pb/U and Pb/Pb isotopic ratios is about 5000. Common ^{206}Pb was corrected using non-radiogenic ^{204}Pb. Pb* is radiogenic Pb.

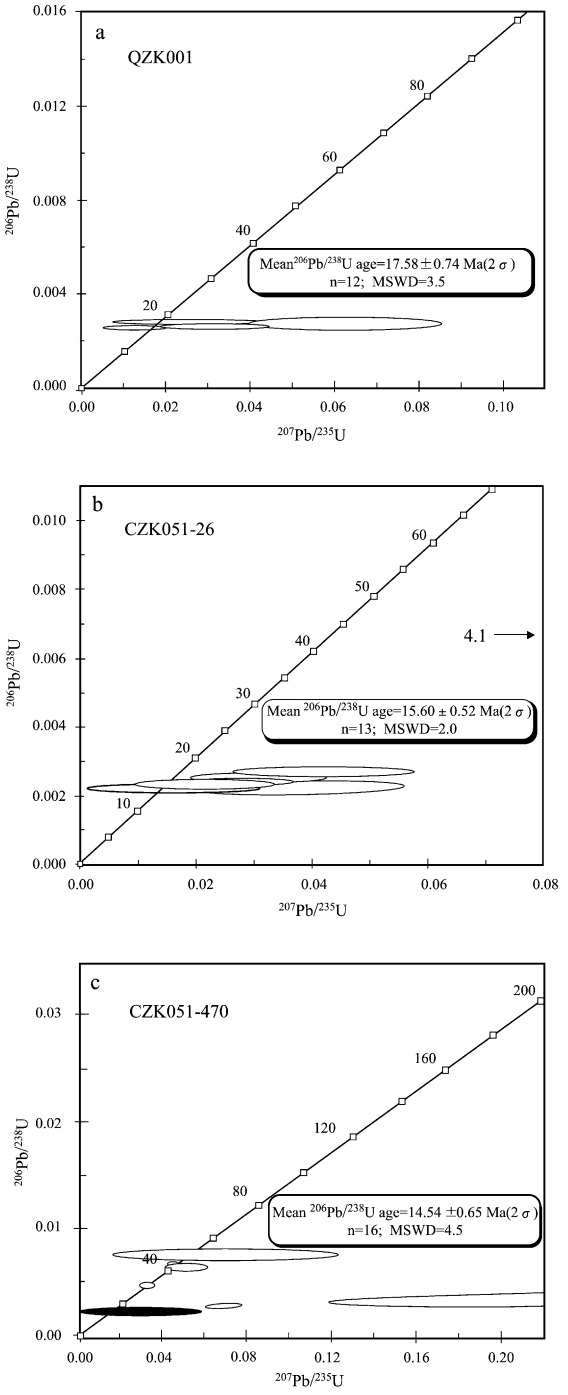

(Table 1). The mean dates for $^{206}Pb/^{238}U$ analyses are used to indicate crystallization age of adakitic magmas, with 95% confidence interval (2σ). The single zircon from the Qulong adakitic rock yielded a weighted mean $^{206}Pb/^{238}U$ age of 17.58 ± 0.74 Ma (2σ). Monzonitic granite–porphyry and diorite–porphyrite at Chongjiang have a single zircon SHRIMP age of 15.60 ± 0.52 and 14.54 ± 0.65 Ma, respectively (Table 1; Fig. 2). Biotite and plagioclase separates from Chongjiang adakitic intrusive yielded $^{40}Ar/^{39}Ar$ plateau ages ranging between 13.5 ± 1.0 and 12.2 ± 0.1 Ma (2σ) [37], which are slightly lower than the zircon U–Pb age, but similar to the bulk rock K–Ar age [35], whereas such separates from Lakang'e adakitic intrusive have consistent plateau ages ranging between 13.4 ± 0.1 and 12.5 ± 1.3 Ma (Table 2). These ages are generally consistent with bulk rock K–Ar ages (16.5–13.4 Ma) for eight fresh adakitic samples from various sites [36], suggesting a cooling duration for these adakitic intrusives to 12–18 Ma, peaking at 16 Ma.

A similar $^{40}Ar/^{39}Ar$ age range has also been reported for the corresponding potassic calc-alkaline lavas, e.g., in the S Gegar and SE Barga (16.2–17.7 Ma [19]), at Maquiang (10–16 Ma [27]) and Gazacun (12.0–13.6 Ma [35]) in south Tibet (Table 2). These available data define a duration of 10–18 Ma for the adakitic magmatism, which is coincident with that of NS-trending ultra-potassic dykes (13–18 Ma), but is later than that of the ultra-potassic volcanism (17–25 Ma) in south Tibet [18,19].

Fig. 3 summarizes major tectonic and magmatic

←

Fig. 2. SHRIMP U–Pb ages of zircons from adakitic intrusives in south Tibet. Quartz monzogranite porphyry at Qulong yielded a mean $^{206}Pb/^{238}U$ age of 17.68 ± 0.74 Ma (2σ) in panel a, in which eight other spots (QZK001-2.1, -3.1, -4.1, -6.1, -7.1, -9.1, -10.1 and -11.1) are not shown. Monzogranite porphyry at Chongjiang gave a mean $^{206}Pb/^{238}U$ age of 15.60 ± 0.52 Ma (2σ) in panel b, in which five spots (CZK051-26-1.1, -3.1, -9.1, -11.1 and -15.1) are not shown. Simple zircon from diorite porphyrite at Chongjiang yielded three groups of $^{206}Pb/^{238}U$ ages (31.0 ± 0.7–41.6 ± 1.2 Ma; 18.4 ± 0.8–23.2 ± 3.3 Ma; 13.0 ± 0.5–16.8 ± 0.4 Ma), the last group gives a mean $^{206}Pb/^{238}U$ age of 14.54 ± 0.65 Ma (16 spots), indicating the magmatic age.

Table 2
Summary of age data for adakitic intrusives and associated volcanic rocks in south Tibet

Location	Rock type	Phase dated	Method	Age (Ma)	Data source
Adakitic intrusives					
East Jiama	Granitic porphyry	Bulk rock	K–Ar	15.9 ± 0.6	[36]
1. Jiama	Granitic porphyry	Bulk rock	K–Ar	15.9 ± 0.5	[36]
		Bulk rock	K–Ar	14.9 ± 0.4	[36]
		Bulk rock	K–Ar	13.4 ± 0.6	[36]
2. Qulong	Monzonitic granite–porphyry	Zircon	U–Pb	17.6 ± 0.7	This study
3. Lakang'e	Quartz monzonitic porphyry	Biotite	$^{40}Ar/^{39}Ar$	13.4 ± 0.1	[37]
		Plagioclase	$^{40}Ar/^{39}Ar$	12.5 ± 1.3	[37]
4. Nanmu	Monzonitic granite–porphyry	Bulk rock	K–Ar	16.0 ± 0.5	[36]
5. Chongjiang	Monzonitic granite–porphyry	Zircon	U–Pb	15.6 ± 0.5	This study
	Diorite porphyrite	Zircon	U–Pb	14.5 ± 0.7	This study
	Monzonitic granite–porphyry	Biotite	$^{40}Ar/^{39}Ar$	13.5 ± 1.0	[37]
		Plagioclase	$^{40}Ar/^{39}Ar$	12.2 ± 0.1	[37]
		Bulk rock	K–Ar	12.2 ± 1.6	[35]
6. Tinggong	Monzonitic granite–porphyry	Bulk rock	K–Ar	16.5 ± 0.8	[36]
Adakitic lavas					
Maquiang	Ignimbrite	Hornblende	$^{40}Ar/^{39}Ar$	15.8 ± 0.8	[27]
		Biotite	$^{40}Ar/^{39}Ar$	14.2 ± 0.2	[27]
		Plagioclase	$^{40}Ar/^{39}Ar$	12.9 ± 0.3	[27]
		Biotite	$^{40}Ar/^{39}Ar$	10.5 ± 0.4	[27]
		Biotite	$^{40}Ar/^{39}Ar$	10.1 ± 0.2	[27]
Gazacun	Ignimbrite	Biotite	$^{40}Ar/^{39}Ar$	13.63	[35]
		Biotite	$^{40}Ar/^{39}Ar$	12.00	[35]
S Gegar	Dacite, rhyolite	Plagioclase	$^{40}Ar/^{39}Ar$	16.2 ± 1.1	[19]
		Biotite	$^{40}Ar/^{39}Ar$	17.7 ± 0.9	[19]
SE Barga	Dacite, rhyolite	Biotite	$^{40}Ar/^{39}Ar$	16.7 ± 0.2	[19]
		Biotite	$^{40}Ar/^{39}Ar$	17.0 ± 0.2	[19]
		Plagioclase	$^{40}Ar/^{39}Ar$	17.0 ± 2.0	[19]

Sites of analyzed adakitic intrusives are shown in Fig. 1b.

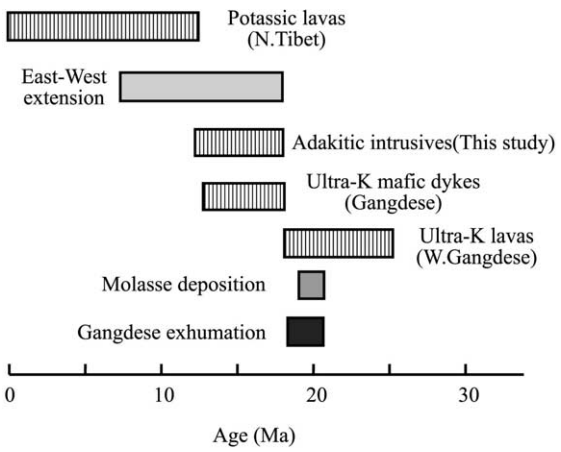

Fig. 3. Age data of adakitic intrusives and age ranges of major tectonic-magmatic events in south Tibet. Age data for adakitic intrusive and extrusive rocks from [19,23,35–37], age range for other tectonic-magmatic events from [18–20,31,38].

events in south Tibet. It seems that the adakitic magmatisms accompanied the east–west extension, and followed the exhumation of the Gangdese batholiths at 18–21 Ma [38] and the molasses deposition at 19–20 Ma [31] in south Tibet. These adakitic intrusives formed in a post-collisional, crustal extension environment.

4. Geochemistry and Sr–Nd–Pb isotopic systematics

The dominant lithologies in the adakitic intrusives are mega-porphyritic monzogranite, quartz monzogranite and quartz diorite, with ~40% modal phenocrystic plagioclase, subordinate quartz, hornblende, and sanidine. They are geochemically shoshonitic, and/or potassic calc-alkaline, similar

to associated potassic calc-alkaline lavas in south Tibet (Fig. 4a; Table 3). All rock types have high silica ($SiO_2 > 64\%$) and aluminum ($Al_2O_3 > 15\%$ at $SiO_2 = 70\%$), but show a range of K_2O content (2.6–8.7%), which is higher than that of adakites produced from slab melting [1]. They usually have relatively high MgO contents (0.6–1.9%; $SiO_2 > 64\%$) and Mg# values (molar [Mg/Mg+Fe]; 0.32–0.74), most of which are more than 0.44, similar to those of adakites from slab melting, but higher than those of the Archean tonalite–trondhjemite–diorite (TTD) [2].

The Gangdese adakitic intrusives are enriched in large ion incompatible elements (Sr: up to 903 ppm; Rb: 41–494 ppm; Ba: 555–1242 ppm), and strongly depleted in high field strength elements (Nb, Ta, Ti), generally showing geochemical features similar to potassic [19] and ultra-potassic lavas [18] erupted since 25 Ma in south Tibet (Fig. 4b). In addition, they have low HREE and Y contents (Yb: 0.94–1.92 ppm; Y: 10.56–19.31 ppm), thus resulting in high Sr/Y and La/Yb values, similar to typical adakites from slab melting (Fig. 4c) [1] and experimental results on partial melting of hydrous basalt in the garnet stability field (Fig. 4d) [1]. Associated Miocene potassic calc-alkaline lavas in south Tibet [18,19] have geochemical characteristics similar to the Gangdese

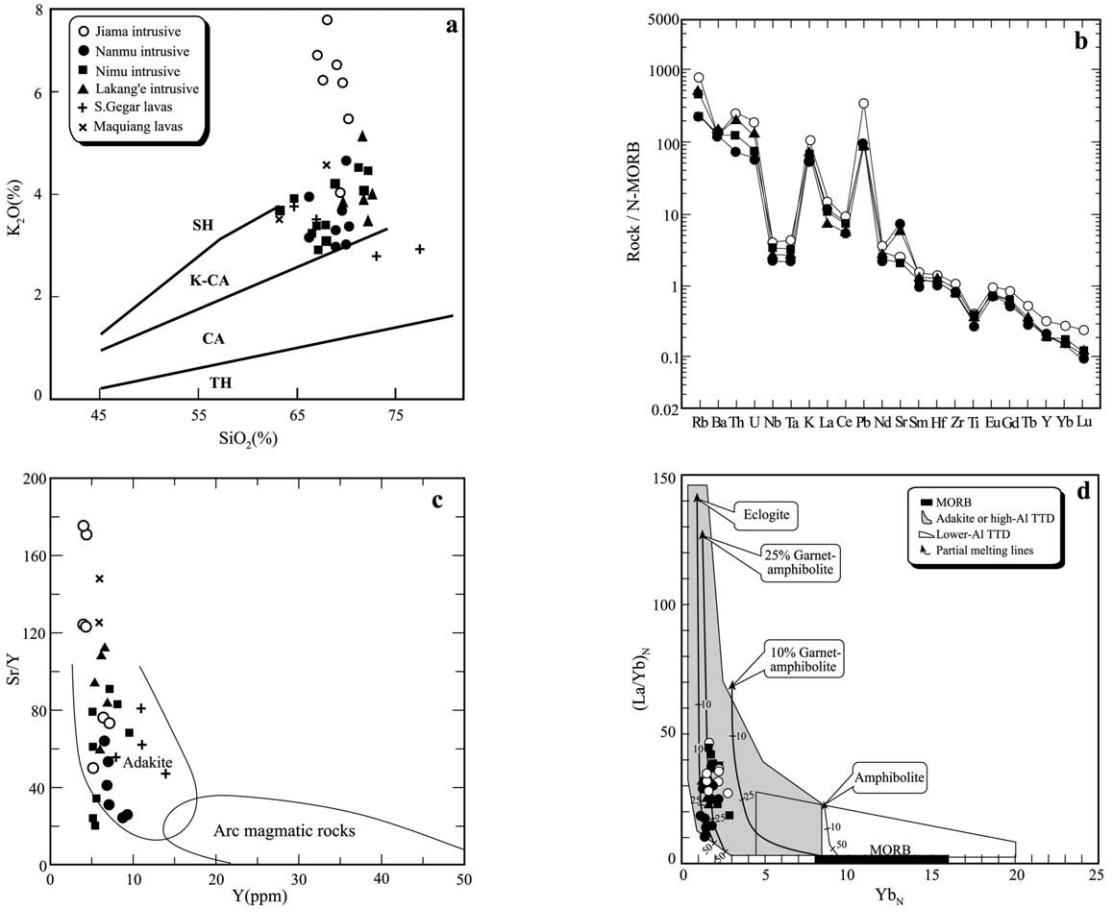

Fig. 4. (a) K_2O–SiO_2 plot of the adakitic intrusives from Gangdese porphyry Cu belts showing they are high-K calc-alkaline and shoshonitic. (b) Normalized abundance patterns of trace elements by N-MORB [58] for the adakitic intrusives. (c) Sr/Y plotted against Y of the porphyries indicating that porphyries from the belt, though having different Y abundances possibly related to composition of the eclogite source, are different from normal arc volcanic rocks and plutons and show adakite magmatic affinity [1]. (d) $(La/Yb)_N$ versus Yb_N diagram for the adakitic intrusives [1]

Table 3
Major and trace element analysis of representative adakitic intrusive samples in south Tibet

	Jiama adakitic intrusives							Lakangé adakitic intrusives				Nanmu adakitic intrusives						
	Jm-7	Jmy-01	Jmy-07	Jm-23	Jm-16	Jmy-04	Jm-21	Dzl-07	Dzl-06	Dzl-05	Dzl-01	Nmy-01	Nty-11	Nty-05	Nmy-02	Nmy-05	Nty-01	Nty-08
SiO_2	68.52	68.59	68.14	68.00	68.29	67.09	69.51	71.51	70.09	71.26	72.42	69.71	70..20	66.94	69.24	69.58	72.18	70..01
TiO_2	0.45	0.39	0.42	0.38	0.37	0.47	0.42	0.29	0.29	0.29	0.30	0.37	0.38	0.45	0.38	0.38	0.30	0.28
Al_2O_3	14.91	14.62	14.44	14.82	14.71	14.62	15.10	15.24	15.78	15.58	15.23	15.33	14.93	15.94	15.78	15.51	14.94	14.64
TFe_2O_3	2.26	1.89	1.85	1.47	1.59	0.98	2.27	088	2.27	1.32	1.56	1.93	2.14	3.11	2.33	3.28	1.07	1.98
MnO	0.06	0.03	0.05	0.04	0.05	0.06	0.07	0.03	0.02	0.04	0.03	0.02	0.02	0.03	0.01	0.02	0.01	0.01
MgO	1.22	1.36	1.41	1.29	1.29	1.43	1.17	0.56	0.66	0.66	0.55	1.15	1.25	1.36	0.81	1.27	0.61	0.61
CaO	1.49	1.88	1.88	2.01	1.30	3.65	0.41	1.77	1.93	2.17	0.82	1.91	1.91	3.06	0.38	0.49	0.34	0.40
Na_2O	3.68	3.32	2.96	2.31	3.25	6.46	3.45	4.07	3.62	4.42	4.30	4.50	4.64	4.39	4.47	4.44	4.45	3.41
K_2O	4.24	6.21	6.55	8.56	7.43	6.68	5.73	4.14	3.61	3.59	4.06	3.43	3.02	3.06	4.37	4.11	4.53	6.57
P_2O_5	0.17	0.17	0.19	0.11	0.17	0.20	0.18	0.09	0.10	0.09	0.14	0.14	0.14	0.18	0.14	0.15	0.05	0.12
H_2O^+	1.47	0.93	1.06	0.42	0.40	0.36	1.21	0.45	0.43	0.10	0.33	1.03	0.94	0.92	1.13	1.15	1.19	1.00
CO_2	0.70	0.14	0.64	0.12	0.58	0.64	0.05					0.05	0.02	0.05	0.58	0.17	0.05	0.11
$Mg^{\#}$	0.52	0.58	0.60	0.64	0.63	0.74	0.51	0.54	0.36	0.48	0.42	0.49	0.54	0.47	0.40	0.52	0.52	0.38
Ba	957	823	930	701	742	796	701	673	691	829	829	989	632	892	1000	789	887	1096
Rb	218	392	380	494	434	424	494	132	91	125	117	97	93.8	97.4	144	137	112	194
Sr	320	444	409	282	239	267	448	570	490	656	348	564	632	903	310	421	428	358
Nb	6.1	7.9	8.3	7.5	7.1	8.0	5.8	6.5	4.9	5.3	6.1	5.0	4.0	4.5	5.1	4.7	5.2	5.3
Ta	0.5	0.7	0.8	0.5	0.5	0.7	0.5	0.3	0.3	0.3	0.4	0.5	0.5	0.5	0.5	0.5	0.5	0.5
Zr	112	106	107	108	111	95	103	40	33	61	51	150	85	115	125	106	84	102
Hf	3.4	3.5	3.5	3.5	3.3	3.0	3.4	1.7	1.4	2.1	2.0	4.4	3.0	3.9	3.9	3.5	3.0	4.0
U	3.3	8.0	8.5	5.8	8.3	7.1	3.3	2.1	1.9	0.3	2.2	0.8	2.2	0.8	1.2	1.4	2.0	0.9
Th	18.3	27.7	25.1	12.0	24.6	26.0	18.9	7.5	6.8	8.6	8.5	9.4	11.6	9.5	13.8	11.1	7.9	11.9
Y	4.6	5.6	5.5	5.5	8.0	6.1	4.1	6.8	5.2	6.0	5.8	5.0	3.4	5.9	3.2	3.4	2.9	3.2
Sc	3.1	3.7	3.9	4.0	3.5	3.9	2.9	3.2	1.9	6.0	2.8	4.8	3.5	5.2	3.8	3.9	3.1	3.2
La	28.77	28.24	25.17	29.50	27.48	31.06	19.68	26.40	17.80	19.40	18.60	17.39	14.19	19.18	6.03	9.03	5.52	8.26
Ce	50.25	48.24	51.64	52.52	44.11	58.63	45.48	55.60	37.80	40.90	37.70	34.40	26.81	40.42	13.98	16.91	11.20	20.8
Pr	6.03	5.66	5.77	5.79	5.50	6.45	4.69	5.78	3.88	4.50	3.97	3.93	2.96	4.89	1.46	1.98	1.35	2.33
Nd	21.93	19.86	19.94	19.44	19.16	22.41	16.69	21.80	14.30	16.60	16.60	14.27	10.65	18.58	5.51	7.28	5.71	8.78
Sm	3.24	3.05	2.98	2.85	2.92	3.35	2.48	2.90	2.29	2.63	2.51	2.45	1.68	3.06	1.06	1.31	1.04	1.50
Eu	0.79	0.73	0.76	0.68	0.71	0.76	0.57	0.94	0.65	0.81	0.69	0.69	0.48	0.84	0.29	0.35	0.29	0.34
Gd	1.88	1.90	1.91	1.83	2.11	2.10	1.48	2.59	1.75	2.01	1.89	1.64	1.06	2.03	0.76	0.87	0.70	0.92
Tb	0.23	0.25	0.25	0.24	0.29	0.27	0.20	0.20	0.17	0.20	0.21	0.21	0.15	0.24	0.11	0.12	0.11	0.12
Dy	1.10	1.22	1.17	1.09	1.51	1.28	0.95	1.45	0.99	1.14	1.08	1.04	0.72	1.19	0.57	0.65	0.53	0.63
Ho	0.19	0.212	0.20	0.21	0.27	0.23	0.16	0.20	0.13	0.16	0.17	0.18	0.13	0.23	0.11	0.12	0.11	0.12
Er	0.48	0.565	0.56	0.53	0.75	0.61	0.42	0.63	0.47	0.53	0.51	0.48	0.35	0.57	0.32	0.35	0.30	0.33
Tm	0.07	0.09	0.09	0.09	0.11	0.09	0.07	0.08	0.06	0.09	0.08	0.08	0.05	0.09	0.05	0.06	0.05	0.06
Yb	0.42	0.537	0.54	0.55	0.69	0.57	0.38	0.55	0.45	0.50	0.47	0.47	0.34	0.53	0.35	0.36	0.34	0.38
Lu	0.07	0.086	0.09	0.09	0.12	0.09	0.06	0.09	0.06	0.08	0.08	0.07	0.05	0.08	0.06	0.06	0.06	0.07
ΣREE	115.38	110.63	111.06	115.4	105.75	127.92	93.29	119.62	80.71	89.48	83.53	77.30	59.62	91.95	30.66	39.44	27.30	44.62
δ Eu	0.98	0.93	0.97	0.90	0.97	0.88	0.90	0.72	0.99	1.08	0.97	1.06	1.10	1.03	0.98	0.99	1.04	0.98
$(La/Yb)_N$	46.51	35.54	31.56	36.31	26.80	36.57	35.09	32.44	30.07	26.22	26.74	25.16	28.37	24.36	11.68	16.81	10.94	14.84
Sr/Y	69.3	79.7	74.1	51.3	29.7	74.1	109.3	84.0	94.6	108.6	59.7	112.7	186.4	152.6	97.8	123.1	146.2	111.9
Y/Yb	11.0	10.4	10.2	10.0	11.6	10.6	10.8	12.4	13.0	12.1	12.4	10.7	10.0	11.1	9.1	9.4	8.6	8.5

Table 3 (*Continued*).

	Nanmu adakitic intrusives							Nimu adakitic intrusives									
	Nmy-04	Nmy-07	Nty-04	PI-18	PI-28	Ng-16	Ng-18	Nt-03	Cj-02	Cj-20	Cj-22	Nt-07	Nt-08	Nt-10	Nt-12	Nt-05	Nt-31
SiO_2	68.75	70.07	71..24	68.43	66.49	68.46	68.79	67.90	68.87	64.90	67.87	67.14	66.83	64.26	68.18	71.19	70.26
TiO_2	0.42	0.36	0.20	0.40	0.57	0.47	0.46	0.49	0.32	0.41	0.35	0.42	0.39	0.58	0.42	0.37	0.39
Al_2O_3	15.79	15.18	14.66	16.30	16.28	15.86	15.76	16.09	14.59	15.38	15.75	15.16	15.12	15.19	15.34	14.99	14.69
TFe_2O_3	1.99	1.45	1.31	2.40	3.77	2.27	2.26	2.16	2.81	3.74	1.98	2.60	2.28	3.12	2.55	1.60	1.63
MnO	0.03	0.02	0.03	0.04	0.01	0.03	0.02	0.01	0.31	0.07	0.09	0.06	0.06	0.06	0.09	0.01	0.02
MgO	1.34	1.09	0.70	0.96	0.85	0.92	0.75	1.49	0.90	0.76	0.82	1.17	1.11	1.93	1.19	0.72	0.90
CaO	1.37	1.08	1.68	2.25	1.07	2.88	2.73	1.53	2.03	3.24	2.40	2.91	2.86	3.38	2.30	0.90	0.72
Na_2O	4.84	3.95	4.24	5.11	3.05	4.80	4.66	4.61	1.63	3.22	3.70	4.13	4.33	3.94	4.69	3.62	3.12
K_2O	3.82	4.93	3.07	2.60	3.33	2.97	3.28	3.51	4.35	4.08	3.18	3.49	3.36	3.63	3.48	4.75	6.01
P_2O_5	0.16	0.13	0.07	0.13	0.22	0.17	0.17	0.19	0.12	0.15	0.13	0.17	0.17	0.23	0.16	0.15	0.18
H_2O^+	0.86	0.97	1.44	0.35	1.75	0.67	0.69	1.14	1.24	1.05	1.13	1.26	1.37	1.61	1.10	1.04	1.07
CO_2	0.17	0.29	1.02			0.05	0.05	0.23				1.05	1.63	0.05	1.02	0.12	0.05
$Mg^{\#}$	0.57	0.60	0.50	0.44	0.32	0.45	0.40	0.59	0.42	0.30	0.38	0.48	0.49	0.55	0.48	0.47	0.52
Ba	884	892	723	785	621	770	787	992	555	711	710	771	813	918	878	868	1206
Rb	134	149	89.9	41	120	51	53	140	280	195	134	144	138	137	112	148	258
Sr	599	501	523	469	500	729	685	686	118	309	290	640	586	637	592	538	388
Nb	5.9	4.5	3.4	6.3	8.0	4. 9	4.6	7.4	6.9	6.9	7.6	7.7	7.7	9.7	7.4	7.2	7.5
Ta	0.5	0.5	0.5	0.3	0.4	0.2	0.2	0.5	0.4	0.3	0.4	0.5	0.7	1.0	0.6	0.5	0.5
Zr	98	88	64	102	102	95	94	146	69	91.6	72.2	148	150	164	158	134	142
Hf	3.4	3.3	2.6	3.0	3.3	2.9	2.9	4.4	2.3	3.0	2.5	4.4	4.4	4.9	4.6	4.0	4.1
U	1.6	1.8	2.4	2.4	3.1	2.2	2.4	2.8	5.9	2.9	4.4	5.3	4.6	4.7	4.1	2.7	6.4
Th	14.4	8.2	5.5	8.5	13.7	7.2	7.1	14.5	14.3	11.4	10.7	22.8	21.9	19.9	16.1	12.4	34.9
Y	4.2	5.0	2.9	6.2	6. 9	4.3	3.9	8.0	5.1	5.1	5.0	6.1	6.2	6.8	5.9	6.6	4.8
Sc	3.8	3.6	2.0	3.1	4.7	2.6	1.8	4.6	3.5	3.5	3.2	3.8	3.8	5.8	4.4	3.3	4.3
La	18.40	15.89	8.64	16.90	33.10	19.60	17.10	19.93	20.90	20.80	18.30	27.70	25.64	29.77	27.81	18.98	26.27
Ce	34.20	28.49	17.00	47.40	64.50	45.70	41.70	53.64	42.00	40.20	45.90	58.27	51.00	67.47	54.03	43.28	46.83
Pr	4.06	3.48	2.09	4.32	7.74	4.84	4.41	6.77	4.68	4.74	4.11	6.26	5.58	7.10	5.65	5.56	5.48
Nd	15.23	12.60	7.70	15.60	29.40	18.90	17.50	25.59	18.10	18.80	16.00	22.51	19.75	25.90	20.35	21.02	19.10
Sm	2.43	2.08	1.27	2.90	4.82	3.08	3.02	4.49	2.97	3.00	2.73	3.57	3.17	4.09	3.23	3.45	2.92
Eu	0.64	0.60	0.35	0.77	1.13	0.84	0.82	1.05	0.77	0.86	0.71	0.87	0.80	1.04	0.81	0.753	0.66
Gd	1.49	1.45	0.85	2.15	3.39	2.08	2.03	2.91	2.08	2.28	1.99	2.25	2.02	2.55	2.06	2.188	1.80
Tb	0.17	0.18	0.11	0.24	0.32	0.20	0.18	0.39	0.21	0.23	0.20	0.31	0.27	0.34	0.28	0.313	0.22
Dy	0.84	0.91	0.53	1.26	1.64	1.02	0.93	1.68	1.12	1.25	1.09	1.40	1.19	1.56	1.36	1.426	0.99
Ho	0.16	0.17	0.10	0.18	0.22	0.12	0.10	0.32	0.14	0.15	0.14	0.23	0.21	0.27	0.23	0.250	0.17
Er	0.40	0.46	0.27	0.61	0.68	0.42	0.36	0.81	0.50	0.51	0.47	0.59	0.54	0.66	0.60	0.654	0.46
Tm	0.06	0.07	0.05	0.06	0.07	0.03	0.02	0.12	0.05	0.04	0.04	0.09	0.08	0.10	0.09	0.096	0.07
Yb	0.41	0.45	0.30	0.60	0.56	0.39	0.33	0.72	0.44	0.44	0.43	0.50	0.46	0.54	0.50	0.552	0.42
Lu	0.07	0.07	0.05	0.06	0.06	0.03	0.02	0.11	0.05	0.04	0.04	0.08	0.07	0.09	0.08	0.0869	0.06
ΣREE	78.54	66.61	39.29	93.05	147.63	97.25	88.52	118.24	94.01	93.34	92.15	124.63	110.79	141.46	117.08	99.14	105.45
δ Eu	1.02	1.06	1.03	0.94	0.85	1.01	1.01	0.88	0.95	1.00	0.93	0.93	0.97	0.98	0.96	0.84	0.88
$(La/Yb)_N$	30.03	23.76	19.72	19.03	39.94	33.96	35.02	18.76	32.09	31.94	28.76	37.29	37.58	37.12	37.51	23.24	42.57
Sr/Y	144.0	99.5	182.3	75.4	72.6	169.9	174.7	85.9	23.2	60.8	58.6	105. 8	95.1	93.2	100.6	81.4	80.6
Y/Yb	10.1	11.1	9.7	10.4	12.3	11.0	11.9	11.1	11.5	11.5	11.5	12.1	13.4	12.6	11.7	12.0	11.6

All analyses were done at the Rock and Mineral Analytical Center, Hubei Geological Bureau (Wuhan). Major elements were analyzed by wet chemistry and XRF, trace elements and REE were analyzed by ICP-AES. Element Ta was determined by ICP-MS at the Geoanalytical Center of Nuclear Industry (Beijing). The routine analytical precision and accuracy for most elements measured are estimated to be $<5\%$. Mg# = 100 $Mg^{2+}/(Mg^{2+}+Fe^{2+})$.

adakitic intrusives, and also show a magmatic affinity with adakite (see Fig. 4) [39–41].

The Nd and Sr isotopic compositions of the Gangdese adakitic intrusives are characterized by a wide range of $\varepsilon_{Nd(t)}$ of 5.52 to −6.18 and $(^{87}Sr/^{86}Sr)_i$ of 0.7050 to 0.7075 (Table 4; Fig. 5a). The low $\varepsilon_{Nd(t)}$ and high $(^{87}Sr/^{86}Sr)_i$ features of some of the intrusives obviously distinguish them from adakites derived from partial melting of subducted oceanic slab (MORB), such as those from Cook Island [40], Adak Island [7] and Cerro Pampa [41]; they generally coincide with the adakitic plutons in the Cordillera Blanca, which were regarded to be derived from partial melting of the lower crust [18]. Compared with the adakitic intrusives, potassic calc-alkaline lavas in the S Gegar have a lower $\varepsilon_{Nd(t)}$ (−7.1 to −9.5) and higher $(^{87}Sr/^{86}Sr)_i$ (0.70903–0.70967), whereas Mayuiyang lavas have a similar Nd–Sr isotopic variation (Fig. 5b). All adakitic intrusives in south Tibet vary between the Yarlung–Zangbo MORB [42] and the Miocene ultra-potassic lavas [18], and fall to the right side of the mixing line between the lower crust (see [18]) and Yarlung–Zangbo MORB (asthenosphere materials) on the $\varepsilon_{Nd(t)}$ versus $(^{87}Sr/^{86}Sr)_i$ diagram (Fig. 5a).

Pb isotopes of the adakitic intrusives are characterized by a wide range of $^{207}Pb/^{204}Pb$ (15.502–15.626) and $^{208}Pb/^{204}Pb$ (38.389–38.960) at relatively invariant $^{206}Pb/^{204}Pb$ (Table 4), forming near-vertical arrays that lie above the northern hemisphere reference line and to the right of the geochron (Fig. 5b). The ends of the arrays point toward modern MORB and the Miocene ultra-potassic lavas, and away from the Yarlung–Zangbo MORBs [42] on the $^{207}Pb/^{204}Pb$ versus $^{206}Pb/^{204}Pb$ diagram (Fig. 5b). The adakitic intrusives have similar $^{206}Pb/^{204}Pb$, but higher $^{207}Pb/^{204}Pb$ than adakites derived from slab melting [7,40,41], suggesting enrichment of radiogenic ^{207}Pb for some of the adakitic intrusives.

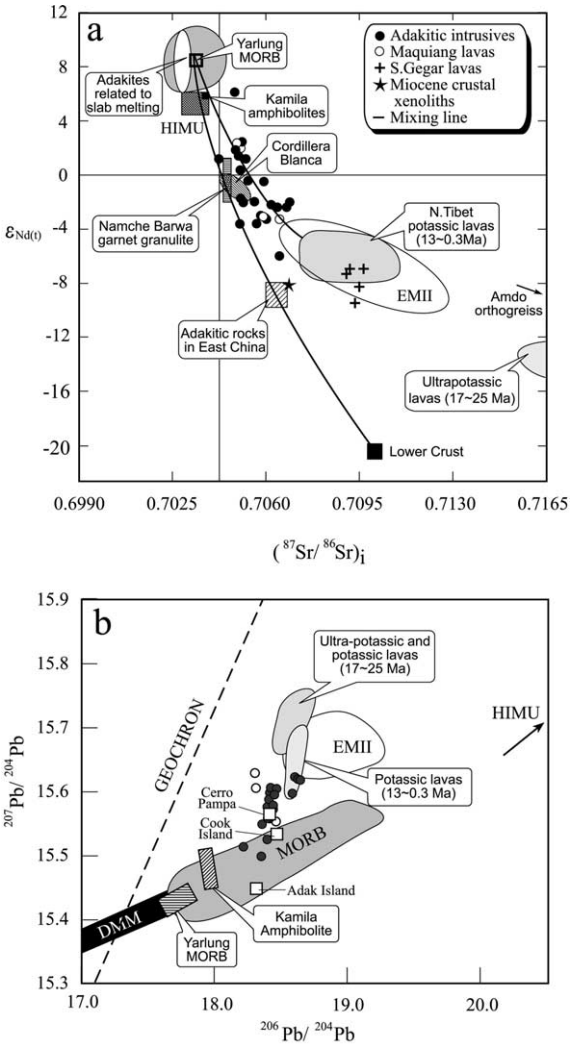

Fig. 5. $^{87}Sr/^{86}Sr$ versus $^{143}Nd/^{144}Nd$ diagram (a) and $^{207}Pb/^{204}Pb$ versus $^{206}Pb/^{204}Pb$ diagram (b) showing the isotopic signatures for the Miocene adakitic intrusives and related potassic calc-alkaline lavas in the south Tibet. Data for lavas from the Gangdese and northern Tibet are from [18] and [19]. In panel a, lower crustal materials in south Tibet are represented by the garnet–amphibolite at Kamila from the western Himalayan syntaxis [47], garnet granulites at Namche Barwa from the eastern Himalayan syntaxis [49], and gabbro xenoliths in the ultra-potassic lavas from the western segment of the Gangdese [18]. Most adakitic intrusives in southern Tibet are in the field, defined by mixing lines between the depleted mantle and lower crust ($^{87}Sr/^{86}Sr = 0.7100$; $^{143}Nd/^{144}Nd = 0.5115$) and between the depleted mantle and enriched mantle (EMII) or the Miocene ultra-potassic lavas in south Tibet [18]. Data for adakitic intrusives from E China [11] and Cordillera Blanca [8] and orthogneiss at Amdo (crustal material) [18] were plotted for comparison. Data for adakites, derived from an oceanic slab, on the Adak Island, Cook Island and Cerro Pampa are from [7], [40] and [41], respectively. DMM, HIMU and EMII represent three types of mantle end-members [59].

Table 4
Sr–Nd–Pb isotopic compositions of the adakitic intrusives in south Tibet

Location	Sample	$\frac{^{87}Rb}{^{86}Sr}$	$^{87}Sr/^{86}Sr$	$\left(\frac{^{87}Sr}{^{86}Sr}\right)_i$	$\frac{^{147}Sm}{^{144}Nd}$	$^{143}Nd/^{144}Nd$	$\left(\frac{^{143}Nd}{^{144}Nd}\right)_i$	$\varepsilon_{Nd(t)}$	$^{207}Pb/^{204}Pb$	$^{208}Pb/^{204}Pb$	$^{206}Pb/^{204}Pb$
Jiama	Jm-16	4.206	0.707920 ± 14	0.7069	0.09424	0.512559 ± 10	0.51254	−1.502	15.626 ± 0.008	18.628 ± 0.009	38.930 ± 0.020
	Jm-23	4.791	0.707360 ± 13	0.7062	0.09189	0.512565 ± 7	0.51255	−1.307			
	Jmy-01	2.238	0.707358 ± 11	0.7068	0.09115	0.512511 ± 6	0.51250	−2.282	15.620 ± 0.008	18.639 ± 0.010	38.924 ± 0.020
	Jmy-04	4.403	0.707536 ± 12	0.7065	0.09272	0.512313 ± 10	0.51230	−6.183	15.618 ± 0.007	18.661 ± 0.008	38.960 ± 0.018
	Jmy-07	2.598	0.707029 ± 10	0.7064	0.07715	0.512517 ± 8	0.51251	−2.088	15.602 ± 0.006	18.599 ± 0.007	38.872 ± 0.016
Lakang'e	Dzl-07	2.031	0.705201 ± 10	0.7047	0.09498	0.512733 ± 6	0.51272	2.010			
	Dzl-06	0.440	0.705163 ± 12	0.7050	0.09825	0.512680 ± 7	0.51266	0.839	15.582 ± 0.009	18.469 ± 0.011	38.587 ± 0.023
	Dzl-05	0.390	0.705146 ± 12	0.7050	0.09520	0.512728 ± 6	0.51271	1.814	15.502 ± 0.011	18.369 ± 0.013	38.389 ± 0.027
	Dzl-01	1.030	0.705444 ± 10	0.7052	0.09987	0.512662 ± 9	0.51265	0.644	15.535 ± 0.010	18.409 ± 0.012	38.478 ± 0.026
Nanmu	Nmy-07	0.760	0.705044 ± 12	0.7048	0.10290	0.512920 ± 10	0.51290	5.520	15.552 ± 0.009	18.381 ± 0.010	38.872 ± 0.016
	Nmy-04	0.561	0.705275 ± 10	0.7051	0.09606	0.51274 ± 12	0.51273	2.204	15.516 ± 0.006	18.227 ± 0.007	38.960 ± 0.018
	PI-18	0.299	0.705064 ± 12	0.7049	0.09453	0.512716 ± 8	0.51270	1.619	15.593 ± 0.017	18.423 ± 0.020	38.567 ± 0.043
	PI-28	0.622	0.705316 ± 10	0.7051	0.09260	0.512651 ± 8	0.51264	0.488	15.612 ± 0.013	18.432 ± 0.015	38.648 ± 0.031
	Ng-16	0.194	0.705126 ± 12	0.7050	0.08179	0.512459 ± 8	0.51245	−3.250	15.575 ± 0.015	18.408 ± 0.017	38.546 ± 0.036
	Ng-18	0.236	0.704907 ± 12	0.7048	0.09399	0.512702 ± 8	0.51269	1.424	15.586 ± 0.009	18.424 ± 0.011	38.520 ± 0.022
Nimu	Cj-02	5.849	0.706424 ± 9	0.7050	0.09176	0.512679 ± 8	0.51266	0.892	15.606 ± 0.008	18.475 ± 0.009	38.721 ± 0.019
	Cj-20	1.586	0.705598 ± 16	0.7052	0.09698	0.512529 ± 8	0.51250	−2.320	15.575 ± 0.014	18.447 ± 0.017	38.561 ± 0.036
	Cj-22	0.760	0.705746 ± 10	0.7051	0.09519	0.512568 ± 8	0.51255	−1.300	15.563 ± 0.017	18.423 ± 0.020	38.543 ± 0.043
	Nt-03	0.566	0.705558 ± 13	0.7054	0.11000	0.512630 ± 8	0.51261	−0.130	15.567 ± 0.016	18.408 ± 0.019	38.609 ± 0.040
	Nt-08	0.598	0.705802 ± 14	0.7056	0.09672	0.512529 ± 6	0.51250	−2.300	15.581 ± 0.006	18.437 ± 0.007	38.620 ± 0.014
	Nt-10	1.383	0.706255 ± 10	0.7059	0.09718	0.512563 ± 10	0.51255	−1.300	15.605 ± 0.010	18.446 ± 0.011	38.695 ± 0.024

Sr–Nd isotopic analysis was done at the Isotope Geology Lab, Chinese Academy of Geological Science (Beijing). Sr and Nd isotopic measurements were done by MC-ICP-MS (MAT-262). NBS987 ratio of $^{87}Sr/^{86}Sr = 0.71025 \pm 2$ (2σ), measurement accuracy of Rb/Sr ratio is better than 0.1%, mass fractionation of Sr isotopes was corrected using $^{88}Sr/^{86}Sr = 8.37521$; J&M ratio of $^{143}Nd/^{144}Nd = 0.511125 \pm 8$ (2σ), measurement accuracy of Sm/Nd ratio is better than 0.1%, mass fractionation of Nd isotopes was corrected using $^{146}Nd/^{144}Nd = 0.7219$. The initial ε_{Nd} values and $^{87}Sr/^{86}Sr$ ratios were calculated at $t = 16$ Ma. Pb isotopic measurements were done by MAT-261 thermal ionization mass spectrometer at the Geoanalytical Center of Nuclear Industry (Beijing). The measurements are accurate to better than 0.05% for $^{204}Pb/^{206}Pb$ and 0.005% for $^{208}Pb/^{206}Pb$ for 1 μg Pb. International standard NBS981 yielded the following results: $^{208}Pb/^{206}Pb = 2.162189$ with an error of 0.0027%; $^{207}Pb/^{206}Pb = 0.913626$ with error 0.0059%; and $^{204}Pb/^{206}Pb = 0.059201$ with error 0.015%.

5. Discussion

5.1. Genesis of the Gangdese adakitic intrusives

Partial melting of subducted oceanic slab is widely regarded as the most internally consistent model for adakite generation, because the geochemical signatures of adakite suggest a basaltic source transformed to garnet amphibolite and amphibole eclogite [1–6]. Other petrogenetic models, such as AFC processes [12] and lower crust melting [8–11], have also been proposed. Castillo [12] emphasized that the AFC processes involving basaltic magma could produce an evolved rock with adakitic composition. However, similar processes seem unlikely to have led to the formation of the Gangdese adakitic intrusives because coexisting Miocene potassic or ultra-potassic mafic and intermediate lavas in south Tibet have much lower $\varepsilon_{Nd(t)}$ (< -12), higher ($^{87}Sr/^{86}Sr)_i$ (≥ 0.7150) (Fig. 5) and higher K_2O contents [18]. Moreover, mafic and/or intermediate lavas parental to adakitic intrusives have not been observed in south Tibet.

The highly enriched N-MORB normalized abundance patterns of trace elements for Gangdese adakitic intrusives (Fig. 4b) suggest the existence of garnet as a residue in the mantle source beneath south Tibet [1,2,43]. The enrichment of Sr and the absence of significant Eu anomalies indicate that the source was plagioclase-free. The element Nb exhibits a tendency to be hosted in amphibole, being at equilibrium with 60–70% SiO_2 melt during partial melting [44], and the element Ti would be hosted in rutile under hydrous mantle conditions [45]. However, both elements are

strongly depleted in the Gangdese adakitic intrusives, which suggests that the source also has residual rutile and amphibole, and thus is most probably garnet-bearing, hydrous garnet–amphibolite or amphibole eclogite [42]. Extreme depletion in Yb and strong fractionation between LREE and HREE suggest that the generation of the adakitic intrusives requires about 10–25% partial melting of the amphibole eclogite or garnet–amphibolite source in south Tibet [1] (see Fig. 4d). This garnet-bearing source implies that there are at least two possibilities for generating the Gangdese adakitic intrusives, i.e., partial melting of thickened lower crust or subducted oceanic slab.

It is expected that the crustal thickening (~70 km) caused by the Asian–Indian continental collision since the Paleocene period will result in the transformation of basaltic lower crust to garnet–amphibolite or amphibole eclogite. In fact, such lower crust materials have been observed in both the western and eastern Himalayan syntaxes on the Tibetan plateau [46–50]. In the western syntaxis, the Paleocene eclogites and associated granulite were exhumed at Babusar Pass in northern Pakistan [47] and at Tso Morari in E Ladakh [48]. Garnet-bearing amphibolites (Kamila amphibolites), interpreted as the basement of the arc, have also been exhumed in the Kohistan arc, the westward prolongation of the Gangdese arc batholith [46]. The Nd, Sr and Pb isotopic compositions of the Kamila amphibolites [49] are similar to those of MORBs derived from depleted mantle (Fig. 5). In the eastern syntaxis, garnet granulite and garnet pyroxenite were exhumed at Namche Barwa [50], and have $^{144}Nd/^{143}Nd$ (0.5125–0.5127) and $^{87}Sr/^{86}Sr$ (0.7044 and 0.7047) (L. Ding, personal communication) values similar to those of adakitic intrusives in the Cordillera Blanca (Fig. 5a). Moreover, lower crustal gabbro xenoliths in the Miocene ultra-potassic lavas in the western segment of the Gangdese arc batholith [18] have a Nd–Sr signature similar to that of adakitic intrusives in East China, which may be derived from lower crust [11] (Fig. 5a). Assuming lower crust has a $^{87}Sr/^{86}Sr$ ratio of 0.7100 and a $^{143}Nd/^{144}Nd$ ratio of 0.5115 (see [18]), these available data indicate that the lower crust samples of the Tibetan plateau fall on or near a mixing line between depleted mantle (MORB) and lower crust on the $\varepsilon_{Nd(t)}$ versus $(^{87}Sr/^{86}Sr)_i$ diagram (Fig. 5a). Simple bulk mixing calculations suggest that the base of lower crust underneath the Tibetan plateau is most probably comprised of asthenospheric materials in various proportions.

Based on the wide ε_{Nd}–ε_{Sr} range for the lower crust in south Tibet, some of the observed Nd–Sr isotopic variations in the Gangdese adakitic intrusives and related extrusive rocks could be interpreted as the partial melts of the mafic lower crust, plus additional input from an enriched mantle or an upper crustal source (see Figs. 4 and 5). Model Nd ages of the Gangdese adakitic intrusives are significantly older than the age of their emplacement, and also suggest crustal origin.

In order to test the possibility of additional input of both upper crustal and enriched mantle sources, we plotted all the available data for potassic adakitic rocks in south Tibet on a Rb/Sr versus La/Ce (Fig. 6a) and a Rb/Sr versus Nb/U (Fig. 6b) diagram. In both diagrams, the Gangdese adakitic intrusives and related lavas show possible derivation from lower crust melting. Nb/U and La/Ce ratios are generally unfractionated during partial melting [51], whereas the Rb/Sr ratio is usually affected by crustal components, thus the trend toward low Nb/U and high La/Ce and high Rb/Sr indicates that upper crust and/or enriched mantle components were involved in the generation of the Gangdese adakitic intrusives. Two groups of these adakitic intrusives can be identified, as shown in Fig. 6. One group, dominated by the Jiama intrusives, is characterized by a high K_2O content (4.24–8.56) and high initial $^{87}Sr/^{86}Sr$ values (0.7062–0.7069). Their Rb/Sr ratios are more than 0.56, higher than that of potassic lavas (13–0.3 Ma) in northern Tibet, but close to that of the ultra-potassic lavas in southern Tibet, suggesting crustal contamination (Fig. 6). Another group, including most of the adakitic intrusives, usually has lower Rb/Sr ratios (<0.50) than those of the ultra-potassic lavas, and varies in the field between adakites from the lower crust and ultra-potassic lavas on the Nb/U versus Rb/Sr diagram (Fig.

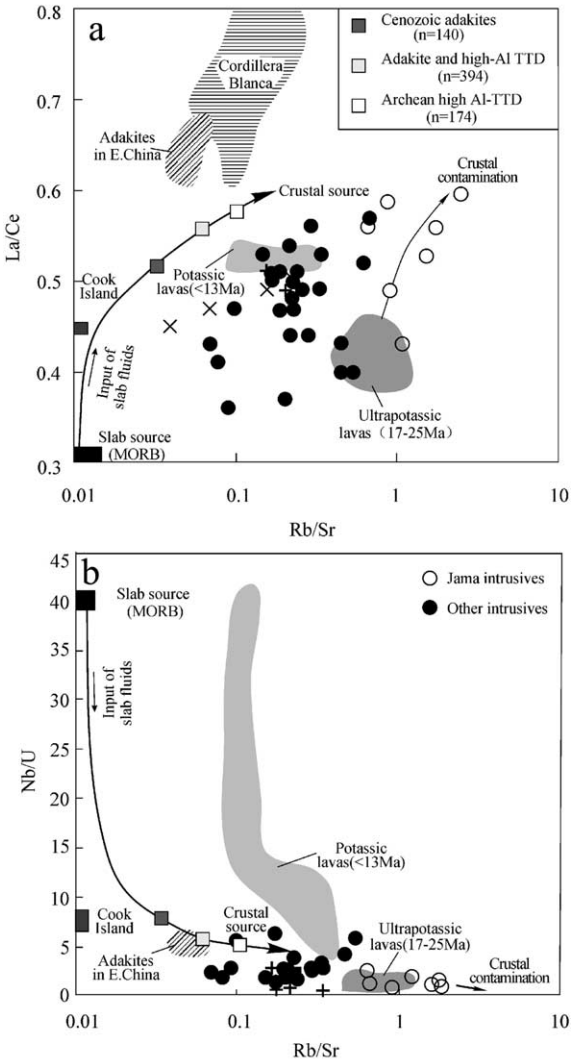

Fig. 6. La/Ce versus Rb/Sr (a) and Nb/U versus Rb/Sr diagram (b) for adakitic intrusives and the Miocene potassic calc-alkaline lavas at Mayuiyang [19] and S Gegar [18]. Adakitic intrusives derived from lower crust are represented by Anjishan rocks in E China [11] and quartz–diorite and tonalite in the Cordillera Blanca [8], respectively. Data for Cook Island adakite derived from oceanic slab are from [40], Cenozoic adakites ($n=140$) predominated slab-derived melts, adakite and high Al TTD ($n=394$) and Archean high Al TTD ($n=174$) derived from lower crust are from [2].

6b), suggesting input of an enriched mantle source (see Section 5.2).

The other candidate for hydrous amphibole eclogite or garnet–amphibolite, that could melt to produce the adakitic intrusives in south Tibet, is the subducted Neotethyan oceanic slab, represented by the Yarlung–Zangbo MORBs. These MORBs have a very limited range of $^{87}Sr/^{86}Sr$ (0.70406–0.70446) and $^{144}Nd/^{143}Nd$ (0.513059–0.513095) [42], which could not be distinguished from adakites derived from slab melting, such as on Cook Island, Adak Island and Cerro Pampa (Fig. 5a). This implies that partial melting of the subducted oceanic slab (MORB) can indeed produce the pristine adakitic melts without additional input of crustal components. Simple bulk mixing of pristine adakitic melts with components from enriched mantle (or ultra-potassic lavas) could account for the observed Sr–Nd isotopic variations in the Gangdese adakitic intrusives, except for the Jiama intrusives, which required additional input from upper crustal materials. However, several lines of evidence, detailed in Section 5.2, do not appear to support this possibility. First, available data for adakites in the world [2] indicate that slab melts generally have Rb/Sr ratios ranging from 0.01 to 0.04, although their Nb/U and La/Ce ratios show much wider variations due to involvement of fluid from a subducted oceanic slab [52]. In contrast, adakites in east China derived from lower crust sources usually have Rb/Sr ratios of >0.05 (Fig. 6). Thus, the high Rb/Sr ratios (>0.05) of Gangdese adakitic intrusives require a large contribution of the lower crust to generate them. Second, the Yarlung–Zangbo MORBs have a much lower $^{206}Pb/^{204}Pb$ (17.63–17.77) and $^{207}Pb/^{204}Pb$ (15.4–15.45) than those of the Gangdese adakitic intrusives; these are inconsistent with the binary mixing mentioned above (Fig. 5b). Third, the Neotethyan oceanic lithosphere was subducted northwards before 130 Ma [53]. An oceanic slab of this age seems unlikely to produce adakitic melts if no additional heat was involved [3]. Moreover, the Miocene adakitic magmatism occurred 35–45 Ma after the Asian–Indian continental collision in south Tibet, and such a delay would not be expected whether flat subduction or incipient subduction of the Neotethyan oceanic slab took place [1,5,6]. Still, our present limited data cannot entirely rule out the possibility of the Neotethys oceanic slab as a source of the adakitic intrusives in southern Tibet.

5.2. Interaction between adakitic melt and enriched mantle

Adakitic magmas, whether derived directly from partial melting of the subducted oceanic slab (MORB) or from lower crustal mafic rocks, usually show characteristics of low Mg (or Mg# value) and high Na rather than high K, as demonstrated by experimental studies [54]. However, the Gangdese adakitic intrusives, though showing some features of typical adakites in arc settings (Fig. 4c,d), have much higher K_2O contents (2.6–8.6 wt%) and Mg# values (0.32–0.74) than adakites. This implies that the K and Mg# anomalies in these rocks were probably formed by processes such as crustal contamination, slab melt/peridotite interaction, binary melt mixing etc., expected during the upward migration of the adakitic melt [9–13].

Crustal contamination could increase K_2O contents in some of the shoshonitic intrusives (Fig. 4a), as suggested by the high $^{87}Sr/^{86}Sr$ and Rb/Sr ratios of the Jiama porphyries (Figs. 4 and 5), but probably cannot account for the observed K_2O and Mg# variation in all the intrusives. The interaction between adakitic melt and peridotite is suggested to be a possible mechanism for increasing the Mg# value of adakites [8,10]. Mixing model calculations using Depaolo's method [55] also indicate that the ε_{Sr}–ε_{Nd} variation of the Gangdese adakitic intrusives could be accounted for by interaction between the enriched mantle (EMII) and the Yarlung MORB (see Fig. 5a). However, the process cannot result in the increase in the K_2O contents of the adakitic melts. An alternative possibility is binary mixing between pristine adakitic melts and enriched mantle-derived melts in variable proportions. Assuming the mantle-derived melt is represented by coexisting ultra-potassic lavas (17–25 Ma [18]) with high Mg# (0.59–0.70 [18]), it is expected that the hybridized melt should have the ε_{Nd}–ε_{Sr} signature and K_2O contents and Mg# values observed in the Gangdese intrusives. This mixing hypothesis is further demonstrated by their near-vertical arrays on the $^{207}Pb/^{204}Pb$ versus $^{206}Pb/^{204}Pb$ diagram (Fig. 5b) and sub-horizontal trends on the Nb/U versus Rb/Sr diagram (Fig. 6b) for most of the adakitic intrusives.

5.3. Tectonic implication

Three significant events characterize the Miocene tectonic and magmatic evolution of south Tibet (Fig. 3). They are: (1) exhumation of the Gangdese batholiths and molasse deposition (18–21 Ma), with associated ultra-potassic and potassic magmatism (17–25 Ma [18]); (2) east–west extension (13.5–18 Ma) that produced NS-trending normal fault systems [20], which in turn controlled the localization of adakitic magmatism peaking at 16 Ma; and (3) widespread, small-volume, potassic volcanism since 13 Ma on the Tibetan plateau [19]. The coincident onset of extensional deformation and appearance of potassic magmatism in south Tibet appears to mark a major change in the tectonic regime. Therefore, any thermal explanation for partial melting of either the thickened lower crust or dead Neotethyan oceanic slab to generate the Gangdese adakitic intrusives must consider these three events.

Radiogenic heating is a possible mechanism for partial melting of mafic materials. However, due to the low thermal conductivity of thickened crust, heating caused by thickening will only be developed on the time scale of the thermal time constant of the lithosphere ($\sim$240 Ma [19]). The thickening of lithosphere and low degrees of extension also rule out the possibility of decompression melting, because the decrease in pressure only resulted in phase transformation of eclogite to granulite in the lower crust, as observed in the eastern Himalayan syntaxis [50]. Another plausible means of attaining enough heat for melting within the continental lithosphere is upwelling of asthenospheric materials by either lithospheric mantle thinning [18,19] or slab breakoff of the Indian plate [21]. Upwelling asthenosphere could cause partial melting of the enriched mantle to produce ultra-potassic magmas [20], which then could pool at the bottom of the lower crust, in turn triggering melting of the lower crustal source. Extremely low V_p (6.91 km/s) and V_s (3.98 km/s) of the lower crustal mafic granulites exhumed at Namche Barwa also suggest that the lower crustal

materials had been evenly heated and melted (Z.-M. Jin, personal communication). The input of components similar to the Miocene ultra-potassic lavas during generation of the Gangdese adakitic intrusives, as suggested by the Nd–Sr–Pb isotopic and trace element data, supports this suggestion.

The convective thinning of lithospheric mantle, as a mechanism for east–west extension [56,57], was regarded as the trigger for partial melting of the Asian mantle and the production of widespread, small-volume, potassic lavas since 13 Ma on the plateau [19]. However, the Gangdese adakitic intrusives and coexisting ultra-potassic lavas were restricted in a 1500 km long, narrow belt along the Yarlung–Zangbo suture. This narrow 'thermal anomaly' belt seems to be easily interpreted by slab breakoff of the subducting Indian plate [21]. According to this model, at ~25 Ma, the breakup of the subducting Indian continental plate was initiated at a depth of about 70–100 km, near the bottom of the lower crust in south Tibet. The hot Indian asthenosphere rose through the broken slab window, and then induced the melting of the lithospheric mantle metasomatized by components of subduction zone to produce ultra-potassic magmas. These magmas, in turn, migrated upwards and triggered the lower crust melting. Based on the above analysis, we conclude that the appearance of the Gangdese adakitic magmatism marked a significant change in geodynamic processes from slab breakoff (25–18 Ma) to convective thinning (18–13 Ma) on the Tibetan plateau. It seems that upwelling and northward movement of the asthenosphere through the broken slab window of the subducting Indian continental plate triggered and promoted the subcontinental mantle thinning on the Tibetan plateau.

6. Conclusions

1. Mid-Miocene adakitic intrusives from south Tibet are the first example of the occurrence of adakites formed in continental collision belts. Close association with mid-Miocene potassic–ultra-potassic lavas and control of NS-striking normal fault systems on localization of such magmas in south Tibet indicate that the collision-type adakite formed in a post-collisional extension environment.
2. These adakitic intrusives are characterized by relatively high K (K_2O: 2.6–8.7%), Mg# (0.32–0.74), and high ($^{87}Sr/^{86}Sr)_i$ (0.7049–0.7079) and low $\varepsilon_{Nd(t)}$ (−6.18–+5.52), compared with adakites produced by oceanic slab melting, which suggests a complex mechanism involving partial melting of mafic materials in a thickened lower crust and the input of enriched mantle and/or upper crust components.
3. Melting of the thickened lower crust in south Tibet requires a significant thermal anomaly, which was most likely triggered by mantle-derived Miocene ultra-potassic magmatism formed by subcontinental mantle thinning or subducted continental slab breakoff.

Acknowledgements

This study was supported by the National Basic Research Plan 973 project (2002CB41260 to Z.Q.H.) from the Ministry of Science and Technology, China. We thank Drs. Chen and Tang for assistance in $^{40}Ar/^{39}Ar$ age measurement and Sr–Nd isotope analysis. The authors benefited from thorough review and constructive comments by Peter Rona and Khin Zaw. We thank Dr. Pat Castillo and Stephane Guillot for many useful reviews that led to many improvements in the paper. ***[KF]***

References

[1] M.J. Defant, M.S. Drummond, Derivation of some modern arc magmas by melting of young subducted lithosphere, Nature 34 (1990) 662–665.
[2] M.S. Drummond, M.J. Defant, P.K. Kepezhinskas, Petrogenesis of slab-derived trondhjemite-tonalite-dacite/adakite magmas, Trans. R. Soc. Edinburgh Earth Sci. 87 (1996) 205–215.
[3] S.M. Peacock, T. Rusher, A.B. Thompson, Partial melting of subducting oceanic crust, Earth Planet. Sci. Lett. 121 (1994) 224–227.
[4] F.G. Sajona, R.C. Maury, M. Pubellier, Magmatic source enrichment by slab-derived melts in a young post-collision

setting, central Mindanao (Philippines), Lithos 54 (2000) 173–206.
[5] M.A. Gutscher, R. Maury, J.P. Eissen, E. Bourdon, Can slab melting be caused by flat subduction?, Geology 28 (2000) 535–538.
[6] B. Beate, M. Monzier, R. Spikings, J. Cotton, J. Silva, E. Bourdon, J.P. Eissen, Mio–Pliocene adakite generation related to flat subduction in southern Ecuador: the Quimsacocha volcanic center, Earth Planet. Sci. lett. 192 (2001) 561–570.
[7] R.W.J. Kay, Aleutian magnesium andesites; melts from subducted Pacific oceanic crust, J. Volcanol. Geotherm. Res. 4 (1978) 117–132.
[8] N. Petford, M. Atherton, Na-rich partial melts from newly underplated basaltic crust: the Cordillera Blanca batholith, Peru, J. Petrol. 37 (1996) 1491–1521.
[9] R.G. Muir, S.D. Weaver, J.D. Bradshaw, G.N. Eby, J.A. Evans, Geochemistry of the Cretaceous Separation Plint batholiths, New Zealand: granitoid magmas formed by melting of mafic lithosphere, Geolog. Soc. J. 152 (1995) 689–701.
[10] C.G. Barnes, S.W. Petersen, R.W. Kistler, R. Murray, M.A. Kay, Source and tectonic implications of tonalite-trondhjemite magmatism in the Klamath Mountain, Contrib. Mineral. Petrol. 123 (1996) 40–60.
[11] J.F. Xu, R. Shinjo, M.J. Defant, Q. Wang, R.P. Rapp, Origin of Mesozoic adakitic intrusive rocks in the Ningzhen area of east China: partial melting of delaminated lower continental crust?, Geology 30 (2002) 1111–1114.
[12] R.P. Castillo, P.E. Janney, R.S. Solidum, Petrology and geochemistry of Camiguia Island, Southern Phillippines: insight to the source of adakites and other lavas in a complex arc setting, Contrib. Mineral. Petrol. 134 (1999) 33–51.
[13] P.R. Rapp, N. Shimizu, M.D. Norman, G.S. Applegate, Reaction between slab-derived melt and peridotite in the mantle wedge: Experimental constrains at 3.8 GPa, Chem. Geol. 160 (1999) 335–356.
[14] Z.-Q. Hou, X.-M. Qu, W. Huang, Y.-F. Gao, The Gangdese porphyry copper belt: the second significant porphyry copper belt in Tibetan plateau (in Chinese with English abstract), Geology in China 28 (2001) 27–29.
[15] X.-M. Qu, Z.-Q. Hou, W. Huang, Is the Gangdese porphyry copper belt the Yulong porphyry copper belt in Tibetan plateau? (in Chinese with English abstract), Miner. Depos. 20 (2001) 355–366.
[16] Z.-Q. Hou, X.-M. Qu, S.-X. Wang, A.-D. Du, Y.-F. Gao, Re-Os age for molybdenites from the Gangdese porphyry copper belt in the Tibetan plateau: implication to mineralization duration and geodynamic setting (in Chinese), Sci. China 33 (2003) 509–616.
[17] Z.-Q. Hou, X.-X. Mo, Y.-F. Gao, X.-M. Qu, X.-J. Meng, Adakite: a significant Cu-bearing porphyry – a case study on porphyry Cu deposits in Tibet and northern Chile (in Chinese with English abstract), Miner. Depos. 22 (2003) 1–12.
[18] C. Miller, R. Schuster, U. Klotzli, W. Frank, F. Purtscher, Post-collisional potassic and ultrapotassic magmatism in SW Tibet: geochemical and Sr-Nd-Pb-O isotopic constraints for mantle source characteristics and petrogenesis, J. Petrol. 40 (1999) 1399–1424.
[19] S. Turner, G. Hawkesworth, J. Liu, N. Rogers, S. Kelley, P.V. Calsteren, Timing of Tibetan uplift constrained by analysis of volcanic rocks, Nature 364 (1993) 50–54.
[20] H. Willams, S. Turner, S. Kelley, N. Harris, Age and composition of dikes in South Tibet: new constraints on the timing of east-west extension and its relationship to post-collisional volcanism, Geology 29 (2001) 339–342.
[21] G. Maheo, S. Guillot, J. Blichert-Tofa, Y. Rolland, A. Pecher, A slab breakoff model for the Neogene thermal evolution of Southern Karakorum and South Tibet, Earth Planet. Sci. lett. 195 (2002) 45–58.
[22] S.-L. Chung, C.-H. Lo, T.-Y. Lee, Y.-Q. Zhang, Y.-W. Xie, X.-H. Li, K.-L. Wang, P.-L. Wang, Dischronous uplift of the Tibetan plateau starting from 40 My ago, Nature 349 (1998) 769–773.
[23] Z.-Q. Hou, H.-W. Ma, K. Zaw, Y.-Q. Zhang, M.-J. Wang, Z. Wang, G.-T. Pan, R.-L. Tang, The Himalayan Yulong porphyry copper belt: produced by large-scale strike-slip faulting at Eastern Tibet, Econ. Geol. 98 (2003) 125–145.
[24] C.-F. Chang, S.-L. Zheng, Tectonic features of the Mount Jolmo Lungma region in southern Tibet, China, Sci. Geol. Sin. 1 (1973) 1–12.
[25] M.A. Murphy, T.M. Harrison, S.B. Durr, Z. Chen, F.J. Ryerson, W.S.F. Kidd, X. Wang, X. Zhou, Significant crustal shortening in south-central Tibet prior to the Indo-Asian collision, Geology 25 (1997) 719–722.
[26] S.B. Durr, Provenance of Xigaze fore-arc basin clastic rocks (Cretaceous, south Tibet), Geol. Soc. Am. Bull. 108 (1996) 669–684.
[27] C. Coulon, H. Maluski, C. Bollinger, S. Wang, Mesozoic and Cenozoic volcanic rocks from central and south Tibet: $^{39}Ar/^{40}Ar$ dating, petrological characteristics and geodynamic significance, Earth Planet. Sci. Lett. 79 (1986) 281–302.
[28] E. Scharer, R.-H. Xu, C.J. Allegere, U-Pb geochronology of the Gangdese (Transhimalaya) plutonism in the Lhasa-Xizang region, Tibet, Earth Planet. Sci. Lett. 69 (1984) 311–320.
[29] A. Yin, T.M. Harrison, Geologic evolution of the Himalayan-Tibetan orogen, Annu. Rev. Earth Planet. Sci. 28 (2000) 211–280.
[30] W.-J. Chen, Q. Li, J. Hao, Postcrystallization thermal evolution history of Gangdese batholithic zone and its tectonic implication, Sci. China 42 (1999) 37–44.
[31] T.M. Harrison, P. Copeland, W.S.F. Kidd, A. Yin, Raising Tibet, Science 255 (1992) 1663–1670.
[32] A. Yin, T.M. Harrison, F.J. Ryerson, Tertiary structural evolution of the Gangdese thrust system, southeastern Tibet, J. Geophys. Res. 99 (1994) 175–201.
[33] M. Coleman, K. Hodges, Evidence for Tibetan plateau uplift before 14 Myr ago from a new minimum age for east-west extension, Nature 374 (1995) 49–52.

[34] P.M. Blisniuk, B. Hacker, J. Glodny, L. Ratschbacher, S. Bill, Z-H. Wu, M.O. McWilliams, A. Calvert, Normal faulting in central Tibet since at least 13.5 Myr ago, Nature 412 (2001) 628–632.
[35] Z.-D. Zhao, X.-X. Mo, S.-Q. Zhang, T.-Y. Guo, S. Zhou, G.-C. Dong, Y. Wang, Post-collisional magmatisms in Wuyu basin, middle Tibet (in Chinese), Sci. China 31 (2001) 20–26.
[36] Xizang Bureau of Geology and Mineral Resources, Regional Geology of the Xizang Autonomic Region (in Chinese), Geological Publishing House, Beijing, 1992.
[37] X.M. Qu, Z.-Q. Hou, Z.Q. Li, $^{40}Ar/^{39}Ar$ ages of porphyries from the Gangdese porphyry Cu belt in south Tibet and implication to geodynamic setting, Acta Geol. Sin. 20 (2003) 355–366.
[38] P.H. Copeland, T.M. Harrison, W.S.F. Kidd, R.-H. Xu, Y.-Q. Zhang, Rapid early Miocene acceleration of uplift in the Gangdese belt, Xizang (south Tibet) and its bearing on accommodation mechanism of the India-Asia collision, Earth Planet. Sci. Lett. 86 (1987) 240–252.
[39] M.J. Defant, M.S. Drummond, Mount St. Helens: Potential example of partial melting of the subducted lithosphere in a volcanic arc, Geology 21 (1993) 547–550.
[40] C.R. Stern, R. Kilian, Role of the subducted slab, mantle wedge and continental crust in the generation of adakites from the Andean Austral Volcanic Zone, Contrib. Mineral. Petrol. 123 (1996) 263–281.
[41] S.M. Kay, V.A. Ramos, M. Marquez, Evidence in Cerro Pampa volcanic rocks for slab-melting prior to ridge-trench collision in Southern South America, J. Geol. 101 (1993) 703–714.
[42] J.J. Mahoney, R. Frei, M.L.G. Tejada, X.X. Mo, P.T. Leat, Tracing the Indian ocean mantle domain through time: Isotopic results from old west Indian, east Tethyan and south Pacific seafloor, J. Petrol. 39 (1998) 1285–1306.
[43] M.J. Defant, P. Kapezhinskas, vidence suggests slab melting in arc magmas, EOS Trans. AGU 82 (2001) 65–69.
[44] J.A. Pearce, M.J. Norry, Petrogenetic implications of Ti, Zr, Y, and Nb variations in volcanic rocks, Contrib. Mineral. Petrol. 69 (1979) 33–47.
[45] Y. Tatsumi, Chemical characteristics of fluid phase released from a subduction lithosphere and origin of arc magma: evidence from high-pressure experiments and natural rocks, J. Volcanol. Geotherm. Res. 29 (1986) 293–309.
[46] Y. Rolland, C. Picard, A. Pecher, H. Lapiere, D. Bosch, F. Keller, The Cretaceous Ladakh of NW Himalaya-slab melting and melt-mantle interacting during fast northwestern drift of Indian Plate, Chem. Geol. 182 (2002) 139–178.
[47] U. Pagnant, D.A. Spencer, First record of eclogites from the Himalayan belt, Kaghan valley, Northern Pakistan, Eur. J. Mineral. 3 (1991) 613–618.
[48] J. de Sigoyer, S. Guillot, J.M. Lardeaux, G. Mascle, Glaucophane-bearing eclogites in the Tso Morari dome (eastern Ladakh, NW Himalaya), Eur. J. Mineral. 9 (1997) 1073–1083.
[49] T. Khan, M.A. Khan, M.Q. Jan, M. Naseem, Back-arc basin assemblages in Kohistan, Northern Pakistan, Geodin. Acta 9 (1996) 30–40.
[50] L. Ding, D.-L. Zhong, A. Yin, T.M. Harrison, Cenozoic structural and metamorphic evolution of the eastern Himalayan syntaxis (Namche Barwa), Earth Planet. Sci. Lett. 192 (2001) 423–438.
[51] A.W. Hofmann, K.P. Jochum, M. Seufert, W.M. White, Nb and Pb in oceanic basalts: new constrains on mantle evolution, Earth Planet. Sci. Lett. 79 (1986) 33–45.
[52] P. Kepezhinskas, F. Mcdermott, M.J. Defant, A.. Hochstaedter, M.S. Drummond, C.J. Hawkesworth, A. Koloskov, R.C. Maury, H. Bellon, Trace element and Sr-Nd-Pb isotopic constraints on a three-component model of Kamchatka arc petrogenesis, Geochim. Cosmochim. Acta 61 (1997) 577–600.
[53] J.C. Aitchison, Badenzhu, A.M. Davis, J.-B. Liu, H. Luo, J.G. Malpas, I.R.C. McDermid, H.-Y. Wu, S.V. Ziabrev, M.-F. Zhou, Remnants of a Cretaceous intra-oceanic subduction system within the Yarlung-Zangbo suture (south Tibet), Earth Planet. Sci. Lett. 183 (2000) 231–244.
[54] R.P. Rapp, E.B. Watson, Dehydration melting of metabasalts at 8–32 kbar: implications for continental growth and crust-mantle recycling, J. Petrol. 36 (1995) 891–931.
[55] D.J. Depaolo, Trace element and combined wallrock assimilation and fractional crystallization, Earth Planet. Sci. Lett. 53 (1981) 189–202.
[56] G.C. Houseman, D.P. McKenzie, P. Molnar, Convective thinning of a thickened boundary layer and its relevance for the thermal evolution of continent convergent belts, J. Geophys. Res. 86 (1981) 6115–6132.
[57] P.C. England, G.A. Houseman, Extension during continental convergence with application to the Tibetan Plateau, J. Geophys. Res. 94 (1989) 17561–17579.
[58] S. Sun, W.F. McDonough, Chemical and isotopic systematics of oceanic basalts: Implications for mantle composition and processes, in: M.J. Norry (Ed.), Magmatism in the Ocean Basins, Geol. Soc. London Spec. Publ. 42 (1989) 313–345.
[59] A. Zindle, S.R. Hart, Chemical geodynamics, Annu. Rev. Earth Planet. Sci. 14 (1986) 493–573.